**Scientia Marina** 82(4)
December 2018, 231-243, Barcelona (Spain)
ISSN-L: 0214-8358
https://doi.org/10.3989/scimar.04801.16A

# Subtidal circulation in a microtidal Mediterranean bay

Pablo Cerralbo [1], Manuel Espino [1], Manel Grifoll [1], Arnoldo Valle-Levinson [2]

[1] Department of Civil and Environmental Engineering, Universitat Politècnica de Catalunya (DECA/UPC), Barcelona, Spain.
(PC) (Corresponding author) E-mail: pablo.cerralbo@upc.edu. ORCID iD: https://orcid.org/0000-0001-7551-0441
(ME) E-mail: manuel.espino@upc.edu. ORCID iD: https://orcid.org/0000-0002-9026-3976
(MG) E-mail: manel.grifoll@upc.edu. ORCID iD: https://orcid.org/0000-0003-4260-6732
[2] Civil and Coastal Engineering Department, University of Florida, 365 Weil Hall, USA.
(AVL) E-mail: arnoldo@ufl.edu. ORCID iD: https://orcid.org/0000-0002-3852-0971

**Summary:** We examine the role of different forcings on the subtidal circulation in a microtidal bay with freshwater inputs in the NW Mediterranean Sea: Alfacs Bay. Observations of subtidal flow in summer 2013 and winter 2014 reveal a two-layered, vertically sheared circulation. During the summer, there is a significant positive correlation between surface currents and winds along the main axis of the bay, while a negative correlation is observed between wind and the bottom layers. During the winter, the cross-shore response is correlated with the most energetic winds, showing a two-layered vertical structure inside the bay and a nearly depth-independent water motion caused by high wind speeds at the bay mouth. The vertical structure of the velocities, as determined through empirical orthogonal function analysis, confirms that surface layers are affected by winds and bottom currents correlated negatively with winds as a response of the wind set-up. Seasonal mean circulation reveals gravitational exchange at the bay mouth during the summer. However, mean circulation is unclear in the inner bay and close to the drainage channels. Observed flow patterns are supported by modelling results that confirm the persistence of averaged current in the low-frequency dynamics. Re-circulation areas in the inner bay indicate the rich spatial variability in flow at low-frequency time scales.

**Keywords:** subtidal circulation; microtidal bay; numerical model; gravitational circulation.

**Circulación submareal en una bahía micromareal del Mediterráneo**

**Resumen:** En esta contribución se examina el papel de distintos forzamientos en la circulación submareal de una bahía micromareal con aportes de agua dulce en el Mediterráneo noroccidental: la bahía de los *Alfacs*. Las observaciones de las corrientes submareales en verano del 2013 e invierno de 2014 muestran una circulación de dos capas con cizalladura vertical. Durante el verano, existe una importante correlación positiva entre las corrientes superficiales y los vientos a lo largo del eje principal de la bahía, mientras que se observa una correlación negativa entre el viento y las corrientes de las capas más profundas. En invierno, la respuesta en la dirección perpendicular a la costa se correlaciona con los vientos más energéticos: con una estructura bi-capa en el interior de la bahía y una circulación prácticamente homogénea en la vertical a causa de la fuerza de los vientos en la zona de la bocana. La estructura vertical de las corrientes se determina a través de análisis EOF y confirma que las capas superficiales están afectadas directamente por los vientos, mientras que las capas más profundas se correlacionan negativamente con los vientos como respuesta del incremento de nivel del mar en la zona más interna debido al empuje de los mismos. La circulación estacional muestra intercambio estuarino en la bocana durante verano. No obstante, la circulación media no es tan evidente en la zona más interna cercana a los puntos de descarga de agua dulce. Los patrones de circulación observados se complementan con los resultados de la aplicación de un modelo numérico que confirma la persistencia de una circulación clara en el domino de la baja frecuencia. Las zonas de re-circulación en la parte más interna de la bahía es una muestra clara de la elevada variabilidad espacial de los campos de corrientes en las escalas temporales de baja frecuencia.

**Palabras clave:** circulación submareal; bahía micromareal; modelo numérico; circulación gravitacional.

**Citation/Como citar este artículo:** Cerralbo P., Espino M., Grifoll M., Valle-Levinson A. 2018. Subtidal circulation in a microtidal Mediterranean bay. Sci. Mar. 82(4): 231-243. https://doi.org/10.3989/scimar.04801.16A

**Editor:** A. Alvera.

**Received:** May 4, 2018. **Accepted:** November 12, 2018. **Published:** December 5, 2018.

## INTRODUCTION

The dynamics and physical processes in estuaries can be investigated at different time scales. A common approach is to use the tidal period as a cut-off frequency and to consider the variability at periods longer than the tides. In most regions, the main tidal currents are semidiurnal (Browne and Fischer 1988) or diurnal (van Maren and Hoekstra 2004). At longer time scales, processes that are due to winds (Noble 1996), co-oscillating waves (Uncles et al. 2014), rain (Grifoll et al. 2011) or intense freshwater inputs (Valle-Levinson et al. 2011) are the main factors controlling the hydrodynamic response. At these scales, processes are categorized as subtidal or low-frequency, and include local wind or remote forced circulation (Janzen and Wong 1998), atmospheric pressure influence (Salas-Monreal and Valle-Levinson 2008) and residual circulation (Narváez and Valle-Levinson 2008). For instance, synoptic events have time scales of two to five days related to the passage time for weather systems and influence the circulation at those scales (Dyer 1997).

The different time scales of winds and density gradients indicate the need to study subtidal flows at those scales. The importance of low frequency on the water environment is therefore great: residence times, as key parameters for evaluating the flow exchange between the open sea and the bay, and the consequent ecological status of the bay, are conditioned by the low-frequency water circulation, among other factors. For instance, the presence of gravitational circulation implies exchange between the estuary and the open sea, thus diminishing the residence time and affecting ecological and biological processes (e.g. Acha et al. 2008, Hagy et al. 2000). Several studies on low-frequency water circulation in a microtidal environments have been made (e.g. Valle-Levinson et al. 2001, Malačič and Petelin 2009), but they are limited by the weak low-frequency flows and the long-term information required.

The main sources of flow variability in microtidal bays (NW Mediterranean Sea, Fig. 1) can be related to winds and seiches at periods shorter than one day (Camp and Delgado 1987, Cerralbo et al. 2014, 2015b). Llebot et al. (2013) showed that wind influences not only the hydrodynamic response but also the hydrographic structures at time scales of a few hours. Therefore, the objective of this contribution is to describe the hydrodynamic response at low frequency in the microtidal and shallow Alfacs Bay. We investigate the mechanisms that force the residual circulation by evaluating the seasonal and spatial variability. Results from a previously implemented numerical model (Cerralbo et al. 2016) provided supplementary information that helped interpret the observations.

## MATERIALS AND METHODS

### Study area

Alfacs Bay is defined as a bar-built estuary (Pritchard 1952) formed by the interaction of Ebro

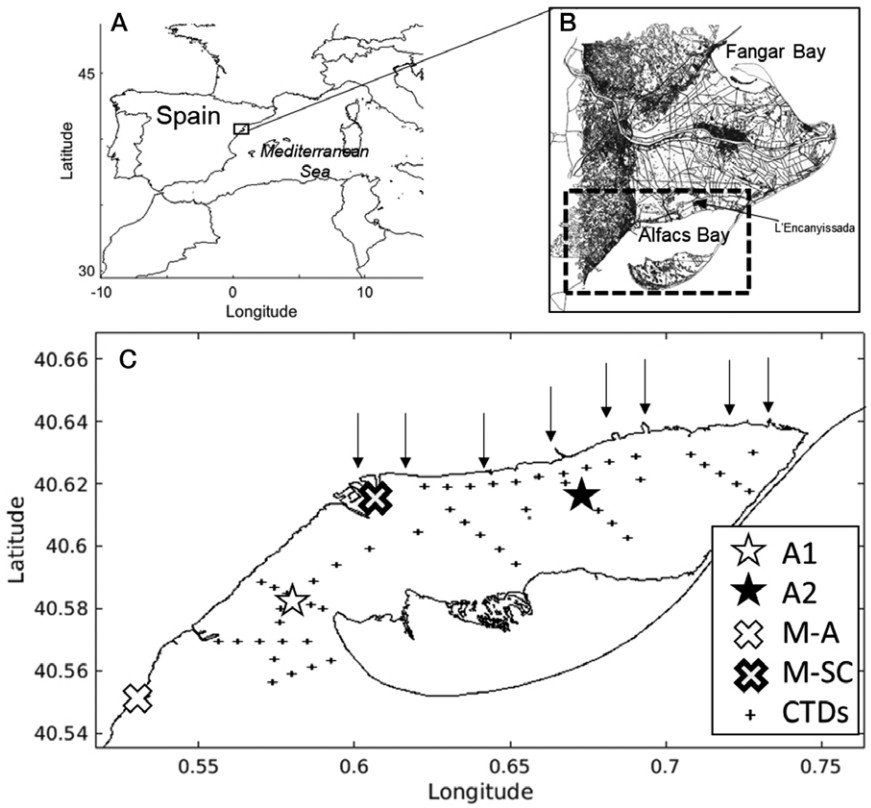


Fig 1. – Alfacs Bay, measurement locations and numerical domain (dashed line in B). The stars indicate the mooring location, the x-symbol specifies the meteorological land-based stations, and the crosses the CTD profiles. The arrows indicate the freshwater discharges from the rice fields used in the numerical model.

River sediment and Mediterranean coastal currents (Fig. 1). The bay is around 16 km long and 4 km wide, with an average depth of ~4 m. Its connection with the Mediterranean Sea is 2.5 km wide, with a central channel with a maximum depth of 6.5 m and shallow shoals of around 1-2 m on both sides. The bay is surrounded by rice fields to the north and a sand spit closing it on the east side. The rice fields contribute around 10 $m^3 s^{-1}$ of nutrient-laden freshwater into the bay from April to December. Alfacs Bay has been defined as a salt wedge estuary for almost all of the year (Camp and Delgado 1987), with a noticeable influence of freshwater fluxes (Llebot et al. 2011, Solé et al. 2009) and heat fluxes during the spring and summer (Cerralbo et al. 2015b). Surface heating and freshwater inputs stratify the bay, promoting the two-layered structure in the water column.

The synoptic winds on the Catalan coast are affected by orographic constraints, such as the blocking winds of the Pyrenees that promote tramontane (N) and mistral (NW) winds over the Ebro Delta area, and the wind channelling due to river valleys (Grifoll et al. 2016). Northerly winds in the region are produced by high pressures over the Azores and lows over the British Isles and Italy (Martín Vide 2005). Winds in the bay have been characterized as having a northwestern and southwestern predominance, with the strongest ones coming from the NW (Cerralbo et al. 2015a).

### Observations

The bulk of the observational data came from two field campaigns: from July to mid-September 2013 and from February to April 2014. The data set consisted of water currents from two 2-MHz acoustic Doppler current profilers (ADCPs) moored at the mouth (A1) and the inner bay (A2). Instruments recorded ten-minute averaged data from ten pings per minute and with 25-cm vertical cells. Both devices were equipped with pressure and temperature sensors, and were mounted on the seabed at 6.5 m depth. Water level data were obtained from the Catalan Meteo-Oceanographic Observational Network (described in detail in Bolaños et al. 2009) in Sant Carles de la Ràpita harbour (M-SC in Fig. 1), and bottom pressure data were from the ADCPs. Atmospheric data (wind, atmospheric pressure, solar radiation and humidity) were obtained from a fixed land station, Alcanar (M-A), and from M-SC. From 2012 to 2014, more than 100 CTD profiles were collected during five intensive daily campaigns. More details on the CTD data are available in Cerralbo et al. (2015b).

In order to analyse the dynamics at low frequencies, both currents and wind observations were filtered using a 30-h low-pass filter (Lanczos filter) (Emery and Thomson 2004). The vertical structure of the water column was investigated using empirical orthogonal functions (EOF) (Emery and Thomson 2004). The EOF analysis was performed considering both along- and cross-shore components at both stations, so that the EOF would explain the combined spatial variability at A1 and A2.

### Numerical model

The three-dimensional hydrodynamic model used in this study is the Regional Ocean Modelling System (ROMS). Numeric aspects are described in detail in Shchepetkin and McWilliams (2005), and a complete description of the model, with documentation and code, is available at the ROMS website: http://myroms.org. The implementation of the model consisted of a regular grid of 186×101 points with a spatial resolution of 100 m (in both the x and y directions) and 12 sigma levels in the vertical dimension. More details about the configuration and validation of the model are described in Cerralbo et al. (2016).

## RESULTS

### Winds

Spectral analysis (Fig. 2A) of wind data from 1996 to 2013 at M-SC (see location in Fig. 1) revealed prominent variance peaks at 24-h and 12-h periods. Both periodicities correspond to sea breezes with strong asymmetry between daily influences (onshore winds) and nightly influences (weaker offshore winds). Lower frequencies contain energy over a broad band. This low-frequency energy is usually associated with the synoptic passage of low-pressure systems, which in the Catalan Sea has periods of 3-12 days (Font et al. 1990).

During the summer, unfiltered data from M-A show a mean wind speed of 3.1 m $s^{-1}$, with a standard deviation of 1.7 m $s^{-1}$ and maximum hourly winds of 13.4 m $s^{-1}$. The sea breeze pattern (diurnal cycle) is clearly observable during the entire summer (Fig. 2B) in unfiltered data, with the exception of two periods of seaward winds. These events occurred on 8 and 25 August and lasted for a few hours (orange box in Fig. 2B, C). In winter, the mean wind speeds rose to 4.2 m $s^{-1}$, with a standard deviation of 3 m $s^{-1}$ and a maximum of 14.2 m $s^{-1}$. On the other hand, the 30-h filtered wind data in summer (winter) showed a maximum of around 6 m $s^{-1}$ (12 m $s^{-1}$). Moreover, in March 2014 more than four events were observed with winds >10 m $s^{-1}$ (Fig. 2D in orange).

### Water current

The filtered depth-averaged current speeds at A1 and A2 (see locations in Fig. 1) are plotted in Figure 2C and 2E for the summer and winter seasons, respectively. The standard deviations are also higher at A1 than at A2 (2.2 and 1.6 m $s^{-1}$ against 1.8 and 1.2 m $s^{-1}$ for summer and winter, respectively). In order to qualitatively compare the wind and current intensities, the filtered wind speeds were scaled by a factor of 0.03. This value corresponds to the theoretical surface layer velocity ($u_w$) due to the wind speed (W), assuming that the relationship follows the quadratic stress law $u_w=(\rho_a/\rho_w)^{1/2}W$ (Large and Pond 1981, deCastro et al. 2003), where $\rho_a$ and $\rho_w$ are the air and water densities, respectively. From 7 to 20 July the depth-averaged water speed response (in both A1 and A2) followed the

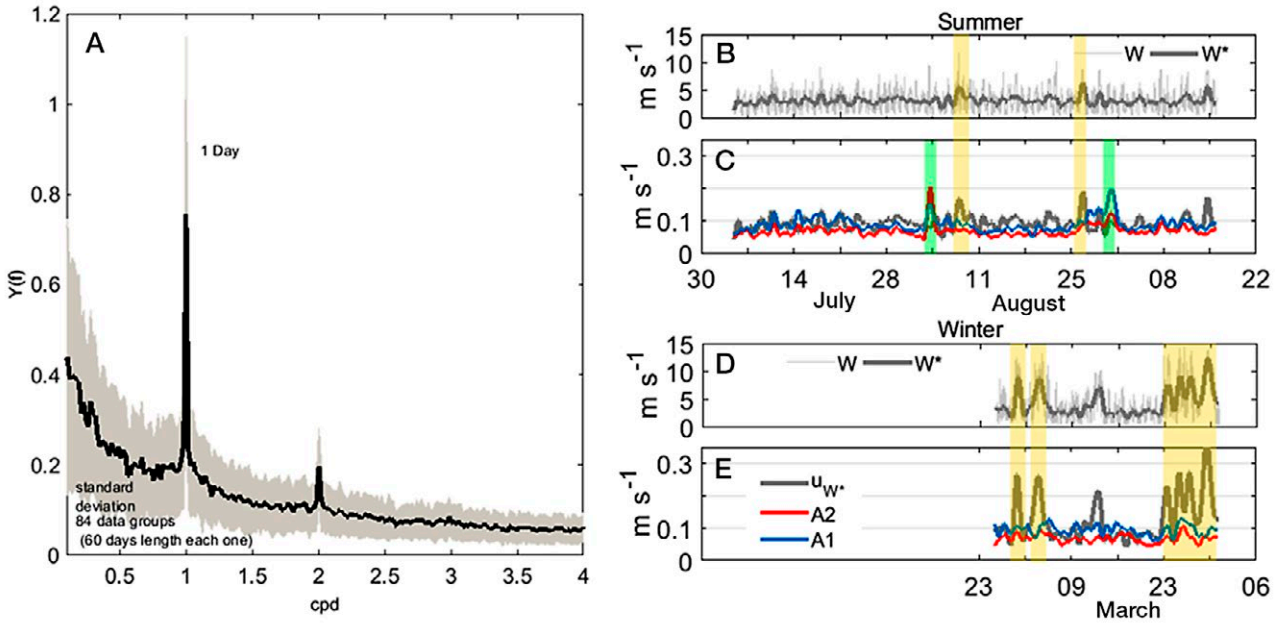


Fig 2. – A, spectral energy for wind observations at M-SC from 1996 to 2013. In order to obtain statistical significance, the data were analysed with a time window of ~60 days (the total amount of 86 data sets being used to obtain the mean and standard deviation). Images B to E show filtered wind (W*) and depth-averaged currents. In B and D, the thin grey line represents wind speed (W) measured at Met-A in summer 2013 and the thick grey line represents 30-h low-pass band filtered wind (W*) in the same period. In C and E, the grey line represents the theoretical surface layer velocity ($u_{w*}$), and the red and blue lines represent the depth-averaged water current speed at A2 and A1, respectively. All units are in m $s^{-1}$.

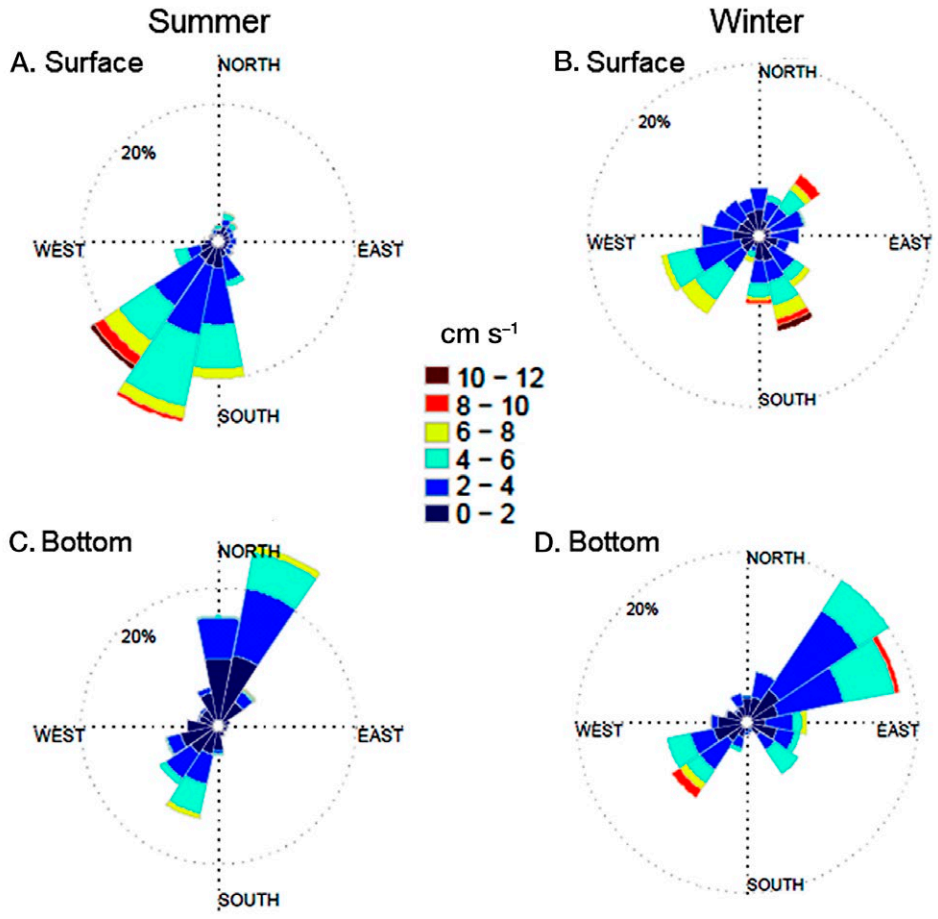


Fig 3. – Current roses for 1-m surface and bottom filtered currents at A1 in summer 2013 (A and C) and winter-spring 2014 (B and D). Both surface and bottom velocities are grouped in a 1-m depth layer. Colour data show the corresponding current speed, grouped in 2-cm $s^{-1}$ intervals and with 16 directions. Units in cm $s^{-1}$.

Table 1. – Correlation coefficients (p-value=0.05) between 1-m surface and 1-m near-bottom averaged currents at the A1 and A2 locations in summer 2013 and winter 2014. Eastward and northward (non-rotated) components are analysed.

| | Summer | | Winter | |
|---|---|---|---|---|
| | A1 | A2 | A1 | A2 |
| R (eastward) | –0.40 | –0.39 | –0.49 | –0.32 |
| R (northward) | –0.72 | –0.21 | –0.09 | –0.24 |

main pattern described by the winds, but for the rest of summer period the graphical comparison in Figure 2C does not reveal a clear relationship between wind and depth-averaged currents. Correlation coefficients between depth-averaged current speeds and winds were close to 0, while in winter their values increased to 0.2 and 0.4 at A1 and A2, respectively. In summer, the maximum current speeds were observed on 4 August, as well as in late August and early September (and with considerable differences between A1 and A2). In both cases, water currents have been related to co-oscillating waves ("seiches") instead of winds or other forcings with hourly time scales (Cerralbo et al. 2014, 2015b). In this case, because the filter is applied on the water speed, the high-frequency signal is not completely filtered and some energy remains in the low-frequency band.

Current rose plots for the filtered currents in the surface and bottom layers (1-m averaged) are shown in Figure 3. In summer, different patterns were observed at each mooring. Seaward flows dominated in the surface layers at A1, and opposite flows in the bottom layers. Meanwhile, at A2 (not shown), inflows dominated in the surface layers. The events with highest current speeds in summer corresponded to NW and NE winds (8 and 25 August, respectively). In winter, the filtered data were more scattered at A1, showing two predominant directions in the surface layers (NE and S-SE), while at A2 (not shown) the surface layers were similar to those observed in summer, although more dispersed from the main axis. The maximum surface velocities at A1 coincided with periods of NW winds (2 to 5 March and 25 March).

Correlations between the surface and bottom layers for both A1 and A2 in both periods are shown in Table 1. At both locations and during all periods, correlations between the bottom and surface layers were negative, indicating the presence of two differentiated layers. In contrast, in winter, the correlation coefficient between

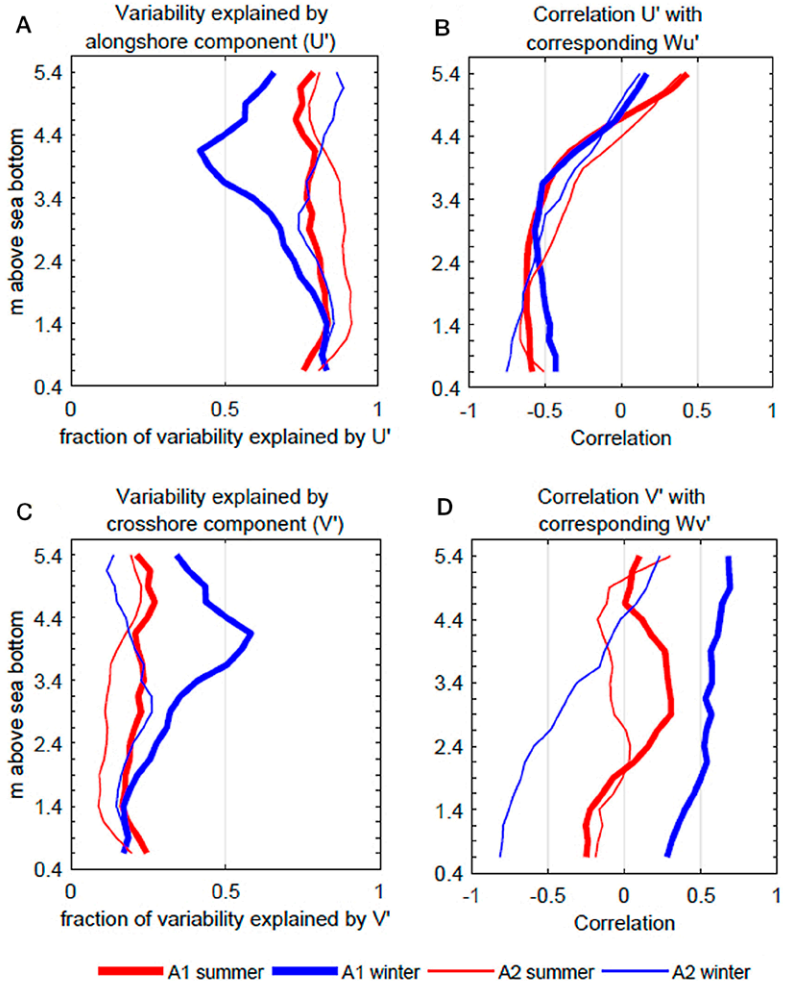


Fig 4. – Left hand side: profiles showing the fraction of variability explained by alongshore (A) and cross-shore (C) components at A1 (thick line) and A2 (thin line) in summer (red) and winter (blue). Right hand side: profiles showing the same components but for the correlation coefficients of each water current layer with wind (panels B and D).

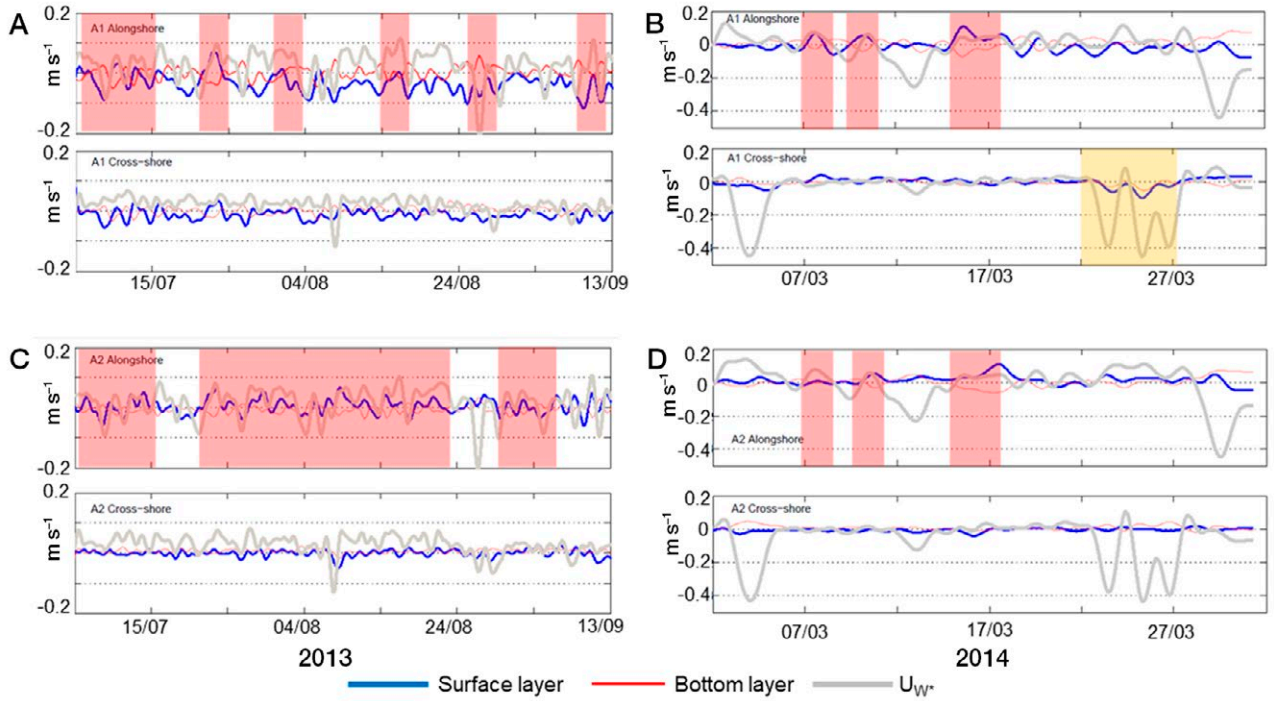


Fig 5. – Summer A1 (A) and A2 (C) filtered time series of $uW^*$, surface (blue) and bottom currents (red). Both wind and currents are plotted following the rotated axis: 21° and 42° anticlockwise for A2 and A1, respectively. Red shaded areas indicate instances of qualitatively relevant correlation between alongshore surface currents and the corresponding winds. Orange shaded areas indicate relevant correlations with the cross-shore currents. Panels B and D show the same parameters in winter.

the surface and bottom layers was ~0 at A1 for the northward component.

## Rotated water currents

Low-frequency current observations show that the maximum variability of the water currents at A1 (Fig. 3) and A2 is associated mostly with one axis aligned with the coastline (following the central axis of the bay). This axis was obtained by adjusting a line (linear regression) between both components (northward and eastward) and obtaining the angle with the east-west axis. Therefore, the explained variability shown in Figure 4A and C expresses the variance of each axis with respect to the total variance. These results are consistent with previous contributions that used unfiltered velocities in Alfacs Bay (e.g. Camp 1994, Cerralbo et al. 2015b). Velocities corresponding to the rotated axis are defined as $u'_{a\_b}$ and $v'_{a\_b}$, with a representing A1 or A2 observations, and b as s or w indicating the summer or winter periods, respectively. The u′ axis corresponds to the along-bay (alongshore) circulation and the v′ axis to the cross-bay (cross-shore) circulation. Alongshore positive values indicate velocities toward the head of the bay. New axes for the filtered data are rotated 20° anticlockwise for A2 for both seasons because the summer and winter observations reveal similar values (19° to 21°). On the other hand, for A1, the axis is 43° anticlockwise in summer. However, winter observations do not reveal a major axis of variability because there are two clearly dominant components (Fig. 3B). For this reason, the rotation for the A1 observations in winter is carried out using the same axis as for the summer observations. In order to compare winds and currents, the wind is also rotated according to the corresponding location.

The variability explained by the new axis for each vertical layer is shown in Figure 4. Alongshore currents accounted for more than 75% of the total variability at A2 in both seasons and at A1 in summer. In winter, the surface layers exhibited a higher variability at A1, indicated by the cross-shore component, as shown by the current rose (Fig. 3B).

The linear correlations between the rotated currents and winds are plotted in Figure 4B and D (considering all water layer depths). There is only a modest correlation of the surface alongshore layer with the corresponding alongshore wind component in summer (R=0.4). In winter, surface currents and winds showed a weak correlation (i.e. ≈0.2), and in all cases this correlation decreased quickly with depth, the sign of the correlation coefficients changing to negative values, with the maximum correlation in the bottom layers (e.g. maximum R=–0.7 in winter at A2).

Considering the limitations of linear correlation coefficients, alongshore and cross-shore currents (both surface and bottom layers) are graphically compared with the corresponding wind components (rotated to the same axis as the currents) for the summer and winter periods in Figure 5. In summer, the results show the maximum wind variability in the alongshore axis. Two energetic events are observed on 8 and 25 August (in green in Fig. 2B). For the currents, the maximum variability is observed in the alongshore direction, with higher speeds in the surface layers. The $u'_{A1\_S}$ shows that 59% of the total speeds are higher than 3 cm $s^{-1}$,

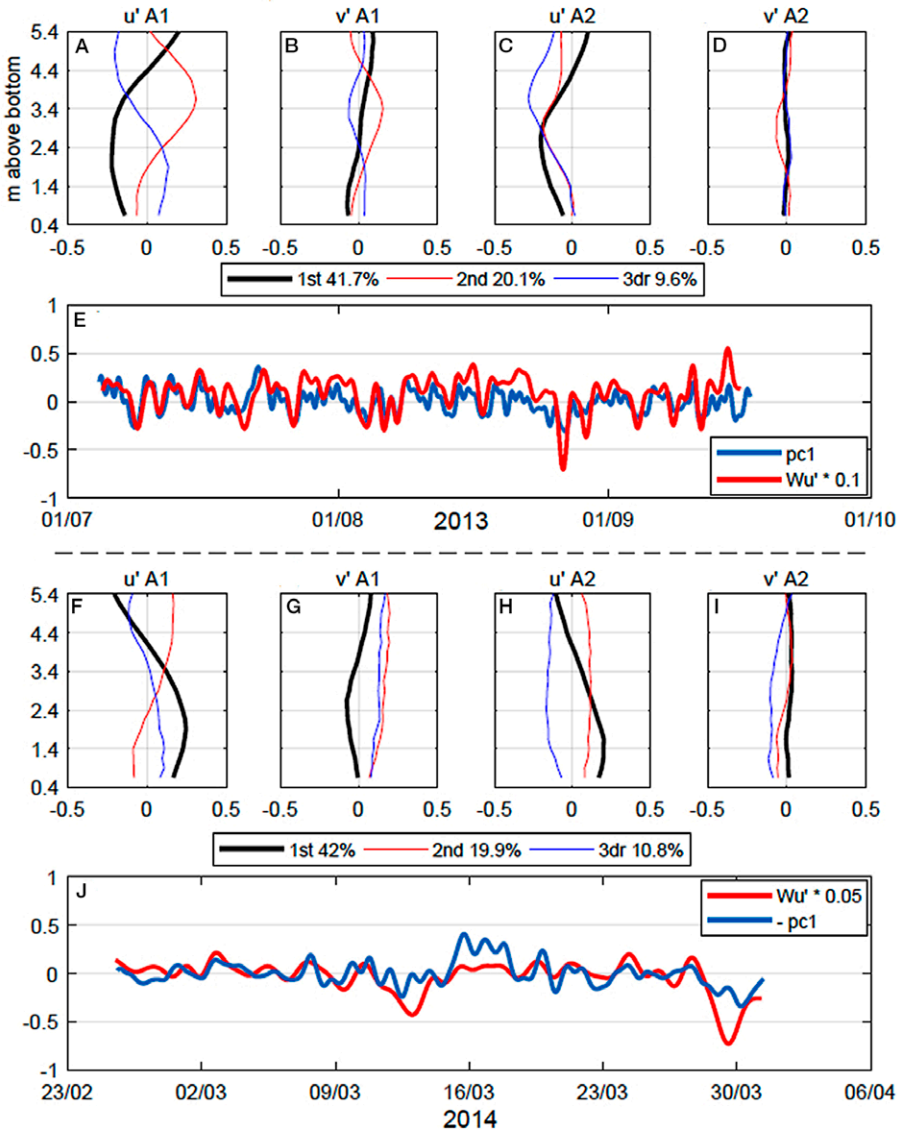


Fig 6. – EOF analysis for low-frequency filtered data (Lanczos low-pass band filter of 30 h) in summer (upper panels) for A1 and A2 alongshore (A and C) and cross-shore (B and D) currents. The legend shows the corresponding percentage of the explained variability. The time evolution for the first component (pc1) is shown in image E, compared with the filtered alongshore wind in red (corrected by factor of 0.1 to improve graphical representation). Images F-J show the same for winter.

while for $u'_{A2\_S}$ only 23% of the total current speeds exceed this threshold. In the cross-shore direction, only 16% and 3% of the observations show values higher than 3 cm $s^{-1}$, respectively. Current velocity in the bottom layers at A2 does not exceed 3 cm $s^{-1}$, and only 14% of the bottom velocities at A1 alongshore exceed this value. Qualitatively, alongshore currents at both A1 and A2 show a clear two-layered structure. In general, at A1 the surface layers show negative values (seaward), reproducing the oscillations observed for the winds, while at A2, the surface currents oscillate between positive and negative values following the main oscillations of the winds. Thus, a relevant surface response to the wind forcing is observed qualitatively on alongshore currents in summer.

In winter, two northerly wind events were observed on 3 to 5 March and 23-28 March (in orange in Fig. 2D). Also, two events of E-NE winds occurred on 13 and 30 March. In general, both the surface and the bottom currents showed the highest alongshore velocities. In early March, there was a direct surface response to two events of SW winds in the alongshore velocities. Between 15 and 17 March, light winds from the SW (aligned with the main axis of the bay) were correlated with surface currents. The most energetic events (northerly winds) did not induce a clear water response at low frequencies in the alongshore velocities. Between 23 and 27 March, both the surface and bottom layers showed a direct response to the wind in their cross-shore components (orange shaded area in Fig. 5B). Using a threshold of 3 cm $s^{-1}$ (as for the summer observations) the measurements at A2 exceeded this velocity 20% and 23% of the time at the surface and the bottom, respectively. On the other hand, at A1, surface layer velocities exceeded 3 cm $s^{-1}$ 44% and 28% of the time. This speed threshold is similar to the observed

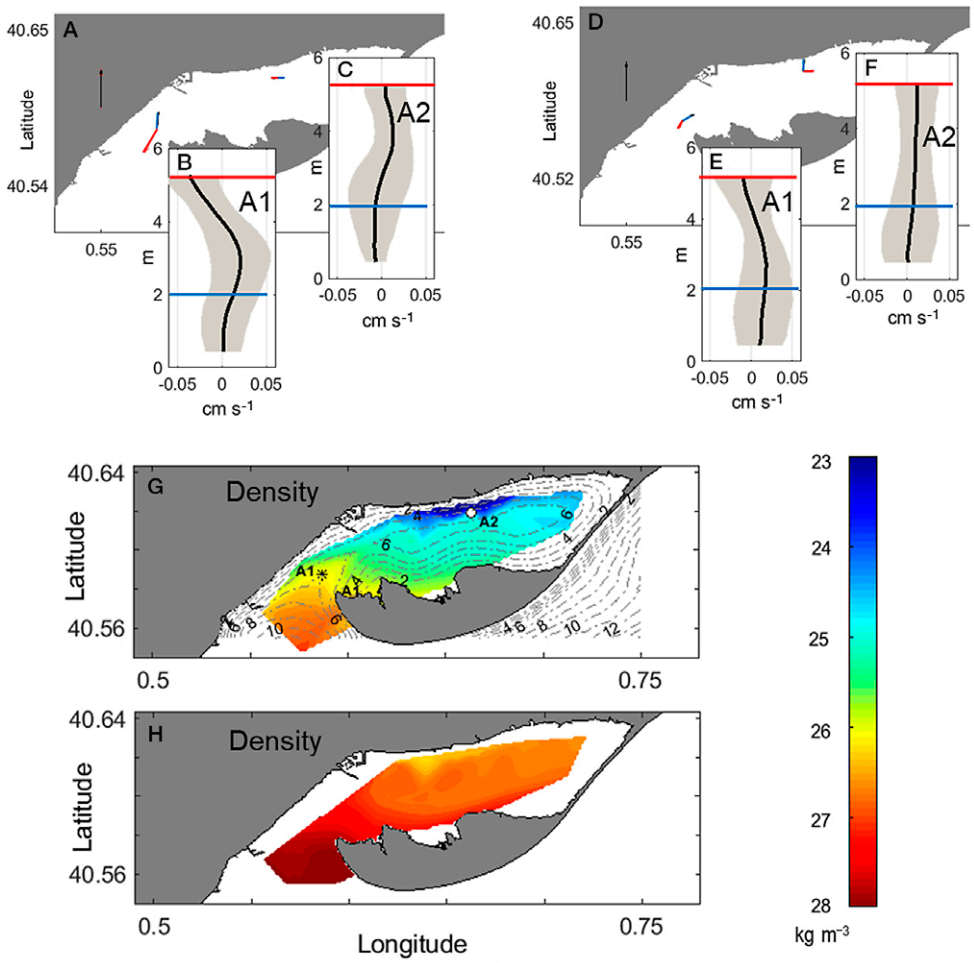


Fig 7. – Residual circulation at A1 and A2 in summer (A) and winter (D) in the surface and bottom layers (red and black, respectively). The respective alongshore velocities along the water column are plotted in B and E for A1, and C and F for A2. The corresponding range (μ±σ) in each layer is shown in grey. The black and blue lines show the surface and bottom layers used to plot averaged velocities in panels A and D. The bottom images (G and H) show the depth-averaged water sigma densities from CTD observations during the field campaigns in May 2014 (G) and February 2014 (H). A black cross shows the location of A1 and a circle that of A2. Isobaths at 1-m intervals are plotted with dashed grey lines.

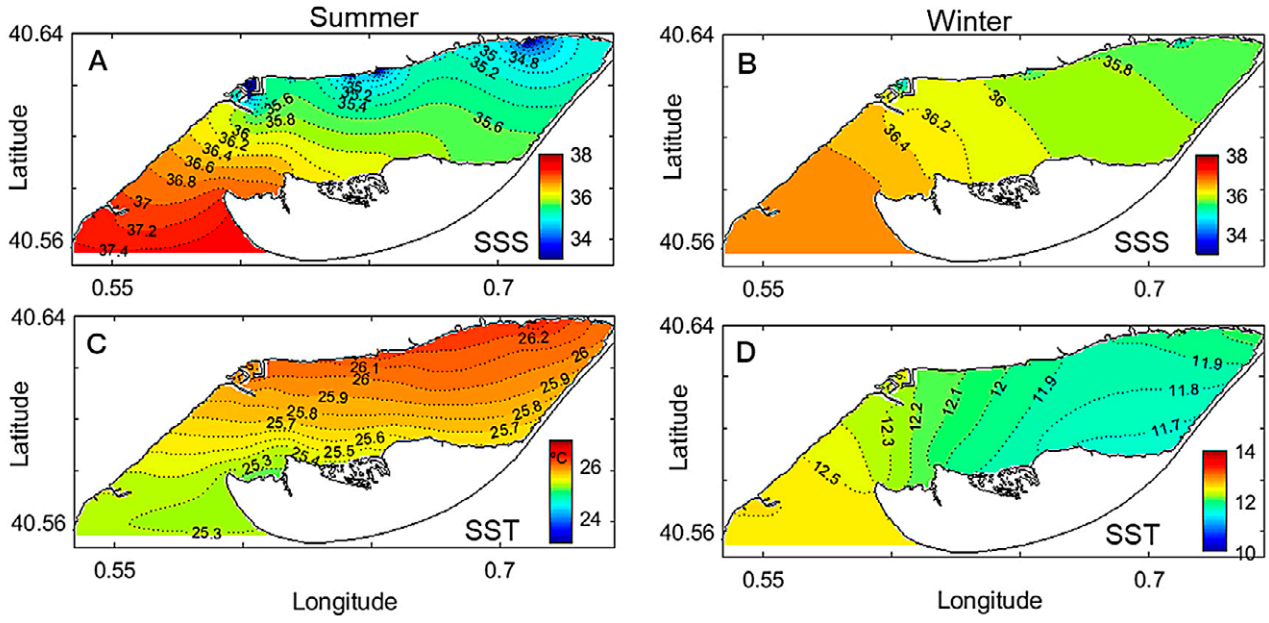


Fig 8. – Left: images for summer simulations (July-September 2013). Right: images for winter simulations. The top images represent the averaged salinity at 0.75 m (SSS) below the surface, and the bottom panels show the sea surface temperature (SST).

standard deviation. Comparisons between currents at A1 and A2 only reveal correlations higher than 0.40 for alongshore components in the surface layers (0.47 and 0.46 in summer and winter, respectively). The maximum correlation was observed in winter in the alongshore component of the bottom layers (0.60).

Along-axis EOF analysis shows differences along both moorings and periods: the first EOF explains 42% in both periods, and reveals a clear two-layered structure (i.e. Fig. 6A-C, F-H), excluding cross-shore at A2 (Fig. 6D, I) with a barotropic response. The second and third EOFs explain ~20 and ~10% of the variability, respectively. In this case, the two-layered structure is only observed in A1 alongshore currents (Fig. 6A, F). The time evolution of the coefficients (PC1, PC2 and PC3) correlates with the alongshore winds (rotated with the same angle as currents at A1). The highest correlation is observed between PC1 and alongshore winds, with values of ~0.66 and ~0.59 in summer and winter, respectively (see Fig. 6E, J). In summer, correlations between the rest of the components (PC2 and PC3) and winds (along- or cross-shore) are not significant. On the other hand, correlation around ~0.5 is observed between PC2 and PC3 with cross-shore winds in winter. Finally, correlations of the first component with currents show maximum values at the bottom layers.

### Averaged circulation (seasonal time scales)

Since gravitational circulation typically occurs over long time scales (weekly and higher), it is instructive to examine the deployment-long mean currents at the moorings (Wong and Valle-Levinson 2002). Averaged circulation for both A1 and A2 was obtained by time-averaging the observations corresponding to the filtered u and v velocities for all measurements in both time periods (summer and winter). The results are summarized in Figure 7. A typical gravitational circulation is observed at A1 during both periods, with outflow at the surface and inflow at depth (Pritchard and Kent 1956). In summer, water currents show southwestward velocities in the surface layers around 4-5 cm $s^{-1}$, and northeastward flows of 2 cm $s^{-1}$ at 2-3 m above the seabed. In winter, the currents are almost in the same direction but at lower speeds. At A2 the situation is completely different. In summer, the surface velocities are very small (close to 0), but in the E-NE direction, while in the lower layers the flow is directed westward at around 1 cm $s^{-1}$. In winter a nearly depth-independent flow is observed at A2, toward the E-NE. The corresponding standard deviations for each averaged current are shown in grey. In general, the variability is higher than the mean value, and only during the summer at A1 do the surface currents show mean values higher than the standard deviation.

## DISCUSSION

### Low-pass analysis

Low-pass filtered velocities revealed a clear two-layered structure, which for 60% to 80% of the time featured opposite directions in the surface and bottom layers. Previous investigations (Cerralbo et al. 2014, 2015b) with unfiltered data showed a one-layered structure for ≈70 % of the time, mostly related to barotropic seiches. In consequence, the removal of these high-frequency oscillations resulted in the predominance of a two-layer vertical structure. Moreover, some additional data analysis using low-pass filters of 6 h and 12 h (not shown) revealed similar percentages to those observed using 30-h cut-off filters. This low-frequency characterization is in agreement with previous studies by Llebot et al. (2013), who observed the predominance of a two-layered structure in averaged circulation.

At A2, the main axis of the bay coincided with the axis of greatest variability in currents in both seasons and was almost equal at all depths (the percentage of variability explained by the first—alongshore—axis was more than 80% for the entire water column). However, A1 showed greater variability in the cross-shore component in winter (mostly in the surface layers), which is related to wind influence. In fact, A1 is 1.5 km from the coast, while A2 is at 600 m. As observed by Noble (1996), close to the shoreline laterally sheared boundary layer currents are expected to flow parallel to the coast. Thus, a transference from cross-shore winds in both locations to the alongshore currents seems clear, as they are higher at A2. A similar example of the strong influence of coastline on water circulation is described in Grifoll et al. (2012).

### Baroclinic circulation

In contrast to a previous EOF analysis with unfiltered flow (Cerralbo et al. 2015b), the current low-frequency EOF analysis showed an evident baroclinic behaviour in alongshore currents at both locations. The first mode (with two-layer structure) explained ~42% of the variability in all cases. These results are similar to those of Llebot (2010), though in their study they suggest that the first baroclinic mode (obtained using weekly time-scale analysis) was related exclusively to gravitational circulation rather than wind forcing. The analysis of the time evolution of each mode is useful to determine possible relationships between physical forcing and the variability described by the EOFs (Salas-Monreal and Valle-Levinson 2008, Schaeffer et al. 2011), even if sometimes the results of EOF analysis may have no physical meaning (Huang et al. 1998; https://climatedataguide.ucar.edu). In our case, the PC1 correlates positively with wind in all periods and locations, linking the main mode to winds (correlations of 0.66 and 0.59 in summer and winter, respectively). On the other hand, cross-shore currents and winds only show relevant correlation or modes 2 and 3 (which explain ~20% and ~10% of variability) in winter, with correlations of around 0.59 and 0.47, respectively. This could be explained by the high winter prevalence of winds aligned with the cross-shore direction.

Similar relevant correlations are observed when filtered winds and surface currents in the along-axis are compared at both locations in summer. However,

in winter, the effects of winds in along-axis surface currents are relatively weak, and the only noteworthy hydrodynamic response is observed in the cross-shore component of A1 during the most intense northwesterly wind. The low-frequency response shows the strongest correlations between winds and bottom currents. Different factors could be responsible for this hydrodynamic response. For example, stratification of the bay modifies the response to wind forcing in the water column. Surface layers are directly affected by wind, while bottom layers respond to the pressure gradient established along the bay due to the wind set-up, as observed in a shallow stratified system by Noble (1996). So, even if the origin is the same (i.e. wind forcing), the current-driving mechanism is different. Surface current observations are restricted to the 1-m layer below the free-surface. Therefore, the oscillations on the pycnocline (close to the surface) may induce a high degree of variability in the water response related to surface winds and the depth of the surface mixed layer. Conversely, bottom layers are farther from the effects of pycnocline oscillation, implying a more stable and consistent hydrodynamic response. Furthermore, the short distances of the observational points from the coast suggest a strong coastline influence (higher at A2), which in turn implies some energy transfer from cross-shore winds to alongshore surface currents.

Another possibility is related to the effects of remote forcing. Winds can induce low-frequency variability in estuaries through a combination of remote and local effects. Considering the remote effect, winds on the continental shelf adjacent to an estuary can produce sea level fluctuations at the estuary mouth (Wong and Valle-Levinson 2002). For instance, variations in the coastal sea level due to the effects of winds (and atmospheric pressure variations) will induce incoming and outgoing flows in the bay. To investigate this phenomenon, we compared the alongshore velocities to the sea level variations and the results shows correlations of 0.6 at the bottom layers and lower correlations (–0.23 to –0.43) at the surface in winter. No correlation was found in summer. These results indicate the possible influence of shelf dynamics in the low-frequency response of the bay, as observed in other environments (Gačić et al. 2004, Murphy and Valle-Levinson 2008, Valle-Levinson et al. 2001). However, more observations on the shelf and numerical experiments covering the Ebro Delta shelf would be necessary to confirm the hypothesis.

At the monthly time scale, the average circulation shows considerable differences from A1 to A2 (Fig. 7). The theoretical gravitational circulation due to freshwater influences (Hansen and Rattray 1965, Pritchard 1952) on the bay would be represented by surface velocities to the west at A2 and to the southwest at A1. Only observations at A1 coincided with the expected gravitational circulation. Moreover, considering some basic statistics such as the standard deviation (Fig. 7), only at A1 and in summer (and especially at the surface) were the averaged currents higher than the standard deviation.

Depth-averaged density fields observed on 7 May 2014 (I-5 campaign) are shown in Figure 7. Two density distribution patterns are observable: 1) in the alongshore direction, from saltier water in the open sea to the freshest water in the inner bay (1027 to 1022 kg $m^{-3}$); and 2) a cross-shore gradient in the inner bay, with the freshest water at the northern margin. Moreover, the freshest water in the north is concentrated around A2, close to the main drainage channels. This density field is representative for the open channel season and similar to that observed in summer 2012 and summer 2013, and to the scenarios described in Camp (1994) and Llebot et al. (2013). Consequently, it seems reasonable to conclude that the average circulation at A1 is explained by the density distributions and differences between inside and outside the bay (considering all freshwater sources in the inner bay), as well as the narrow shape of the bay mouth.

Another factor to consider is the wind stress influence on the gravitational circulation. Several reversals of surface flows have been observed in previous studies (Llebot et al. 2013, Cerralbo et al. 2015b). On those occasions, the wind stress overwhelmed the gravitational circulation. The competition between wind stress and density gradients to produce subtidal flows is characterized with the Wedderburn number W (e.g. Monismith 1986, Valle-Levinson and Blanco 2004):

$$W = \frac{\tau_s L}{g \ \rho h^2}$$

with L being the basin length (around 16 km), g the gravity acceleration (9.81 m $s^{-2}$), $\Delta\rho$ the density difference between two points, h the depth, and $\tau_s$ the surface wind stress. The wind stress $\tau_s$ is computed following Large and Pond (1981) as $\tau_s = C_d \rho_{air} U^2$, where $C_d = 1.3\ 10^{-3}$, $\rho_{air} = 1.22$ kg $m^{-3}$, and U is the wind speed. Using W~1, we can obtain the theoretical threshold for overcoming the gravitational influences by wind stress. The only unknown value is the corresponding density gradient. Considering the depth-averaged density fields shown in Figure 7, density differences between the inner bay and the open sea in summer are around 3-5 kg $m^3$. These values suggest that winds of between 4 and 5 m $s^{-1}$ would be able to overcome the gravitational circulation. This analysis therefore gave us a general picture of the bay behaviour, but no specific description of responses at A1 and A2.

A2 is located in the middle of the bay and close to drainage channels. Thus, if the bay is divided into two areas from a cross-sectional axis at A2, freshwater inputs are distributed on both sides, diminishing (even cancelling) the possible gravitational circulation along the main axis of A2. This means that the average circulation in the along-axis direction at this point is likely to be more influenced by other factors, but mainly wind forcing.

## Spatial variability: modelling study

The spatial variability of the mean circulation in the bay is illustrated with the results from a numerical model (Figs 8-9). Modelled average salinity and tempera-

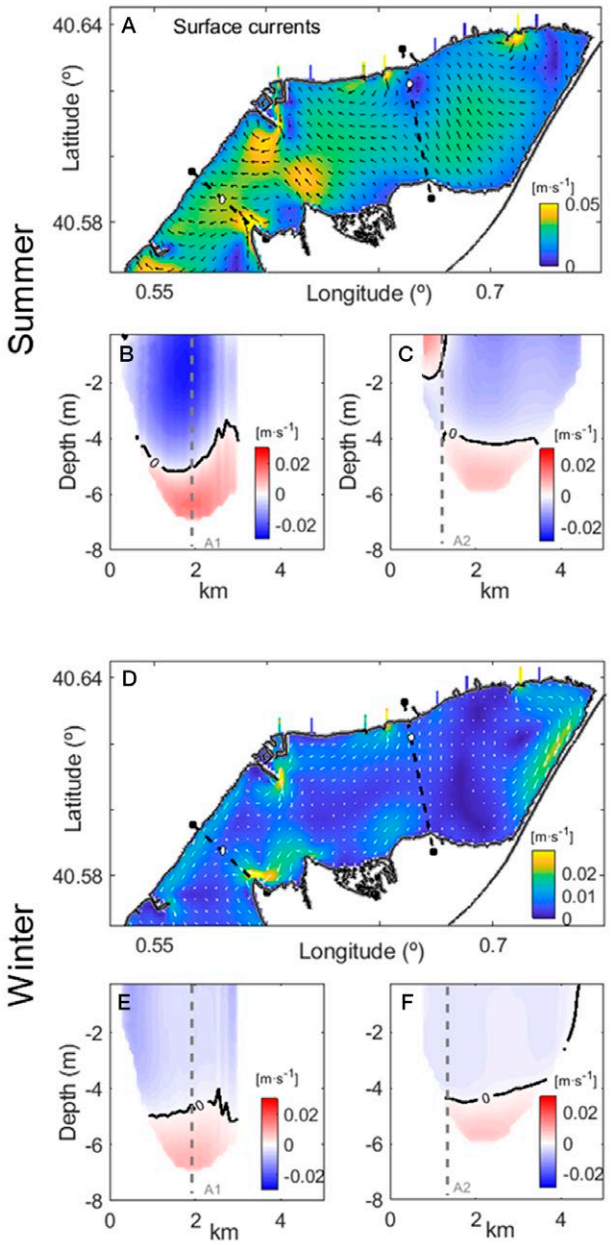


Fig 9. – Top images (A and D) show the modelling results for the average circulation in summer 2013 (A) and winter 2014 (D). Flows across the black dashed sections (A and D) are plotted in images B and C for summer, and E and F for winter. Locations of the ADCP moorings are shown with grey circles.

ture fields (Fig. 8) revealed similar structures to those described by observations. For example, the modelled surface 2D salinity fields are very similar to the density structures observed in May 2014 (Fig. 7G). Moreover, the modelled salinity during the closed channels season (Fig. 8) shows a similar structure to that observed and described in Figure 7H, and previously described by Camp (1994), with density gradients along the bay and a well-mixed water column (not shown). Averaged surface currents in summer (Fig. 9A) show maximum velocities located close to the bay mouth. On the other hand, modelled velocities at A2 are much weaker than at A1, agreeing with observational data, with the directions also showing same vertical variability. As stated above, A2 is more sensitive to the freshwater inputs and the influence of winds, which influence the density-driven circulation.

Moreover, numerical results show how the near-surface average circulation exhibits two different behaviours inside the bay. The inner area (from A2 to the head of the bay) describes a near-surface anticyclonic circulation that follows isobaths. This behaviour was more evident in winter and related to spatial variability of northwesterly winds and bathymetry (Cerralbo et al. 2016). On the other hand, from A2 to the bay entrance, the main surface currents are seaward, consistent with the classical gravitational circulation. Also, in winter (Fig. 9D-F) relatively lower velocities appeared throughout the bay, and the maximum averaged velocities occurred at the margins (in the shallower areas). Moreover, two different structures are visible: the clearest being an anticyclonic gyre in the inner bay (close to the head), which clearly separates the average circulation from the region close to the bay mouth. These patterns suggest weak connectivity between the two bay volumes, and this disconnection would imply differences in residence times in the bay.

In summer, flows perpendicular to the cross sections (Fig. 9B, C) reveal two-layer exchange with the interface at a depth of 3-4 m. The maximum outflows in the bay mouth are at the centre of the section (3 cm $s^{-1}$) and the maximum inflows are at the bottom. However, the inner bay flows also display horizontal shears over the shallower area close to the channels (also shown by the observations in Fig. 7C). This zone is located between the main freshwater discharge points and the surface anticyclonic circulation. During the winter, there is also a two-layered circulation in both sections. However, in winter the maximum outflows (1 cm $s^{-1}$) are located over the margins, while outflows are almost null in the centre of the bay.

The summer results revealed that during that season the average behaviour of the bay seems to predominate over the variability at this time scale (low frequency, with a cut-off time of 30 h). This dominance is clearer at the bay mouth, and probably directly correlated with the gravitational circulation. In winter, the average circulation is not as evident as in summer, and the variability dominates over the mean behaviour in the shallower areas.

## CONCLUSIONS

Analysis of the flow structures in the bay and their variability, through EOF, revealed a clear two-layer response at low-frequency scales (>30 h). Observations indicated a positive relationship between surface currents and winds along the main axis of the bay in summer and winter, while negative correlation is observed in the bottom layers. On the other hand, in winter the cross-shore flow responds to winds at the bay mouth, showing one-layer flow. In winter, significant correlation coefficients between alongshore winds and bottom alongshore currents (negative values) indicate that the near-bottom currents in the bay respond to a wind set-up.

At much longer time scales (monthly), averaged circulation reveals gravitational circulation at the bay mouth, only noticeable in summer. In the inner bay (A2), and close to the drainage channels, no clear averaged circulation is observed (low velocities) and variability induced by wind stress and proximity to the coast is greater. Observations show that density structure within the bay may be responsible for this behaviour. Observed patterns are supported by modelling results that make it possible to estimate the spatial variability of averaged currents in the low-frequency dynamics. Re-circulation areas in the inner bay suggest the need for further studies in order to understand the influence of spatial variability on spatial distribution of nutrients and sediments.

Finally, both wind-induced and gravitational circulation are evident at the low-frequency band. Although gravitational circulation is prevalent in summer due to the persistence of the density gradients, episodic onshore winds alter this pattern (i.e. there are reversals in the estuarine circulation due to sea breezes).

## ACKNOWLEDGEMENTS

We want to thank Joan Puigdefàbregas, Jordi Cateura and Joaquim Sospedra from the Maritime Engineering Laboratory (LIM/UPC) for all their help with campaigns and data analysis, and the XIOM network for the information provided. The campaigns were carried out thanks to the MESTRAL project (CTM2011-30489-C02-01). The authors also acknowledge the funding and support received from the Direcció General de Pesca i Afers Marítims in the framework of the project "Anàlisi ambiental de les Badies del Delta de l'Ebre i el seu entorn. Cap al desenvolupament d'una eina per a la seva gestió integrada" and the ECOSISTEMA project (CTM2017-84275-R). We also want to thank the Secretariat for Universities and Research of the Ministry of Economy and Knowledge of the Generalitat of Catalonia (Ref 2014SGR1253), who supported our research group.

## REFERENCES

Acha E.M., Mianzan H., Guerrero R., et al. 2008. An overview of physical and ecological processes in the Rio de la Plata Estuary. Cont. Shelf Res. 28: 1579-1588. https://doi.org/10.1016/j.csr.2007.01.031

Bolaños R., Jorda G., Cateura J., et al. 2009. The XIOM: 20 years of a regional coastal observatory in the Spanish Catalan coast. J. Mar. Syst. 77: 237-260. https://doi.org/10.1016/j.jmarsys.2007.12.018

Browne D.R. Fisher C.W. 1988. Tide and tidal currents in the Chesapeake Bay. NOAA Tech.l Rep. NOS OMA 3, Rockville, MD, 84 pp. plus appendices

Camp J. 1994. Aproximaciones a la dinamica estuarica de una bahia micromareal Mediterranea. Ph.D. thesis. Univ. Barcelona.

Camp J., Delgado M. 1987. Hidrografia de las bahías del delta del Ebro. Inv. Pesq. 51: 351-369.

Cerralbo P., Grifoll M., Valle-Levinson A., et al. 2014. Tidal transformation and resonance in a short, microtidal Mediterranean estuary (Alfacs Bay in Ebre delta). Estuar. Coast. Shelf Sci. 145: 57-68. https://doi.org/10.1016/j.ecss.2014.04.020

Cerralbo P., Grifoll M., Moré J., et al. 2015a. Wind variability in a coastal area (Alfacs Bay, Ebro River delta). Adv. Sci. Res. 12: 11-21. https://doi.org/10.5194/asr-12-11-2015

Cerralbo P., Grifoll M., Espino M. 2015b. Hydrodynamic response in a microtidal and shallow bay under energetic wind and seiche episodes. J. Mar. Syst. 149: 1-13. https://doi.org/10.1016/j.jmarsys.2015.04.003

Cerralbo P., Espino M., Grifoll M. 2016. Modeling circulation patterns induced by spatial cross-shore wind variability in a small-size coastal embayment, Ocean Model. 104: 84-98. https://doi.org/10.1016/j.ocemod.2016.05.011

deCastro M., Gómez-Gesteira M., Prego R., et al. 2003. Wind influence on water exchange between the ria of Ferrol (NW Spain) and the shelf. Estuar. Coast. Shelf Sci. 56: 1055-1064. https://doi.org/10.1016/S0272-7714(02)00302-5

Dyer K.R. 1997. Estuaries: A physical introduction. Wiley, New York, 195 pp.

Emery W.J., Thomson R.E. 2004. Data Analysis Methods in Physical Oceanography. 2nd ed. Elsevier, 638 pp.

Font J., Salat J., Julià A. 1990. Marine circulation along the Ebro continental margin. Mar. Geol. 95: 165-177. https://doi.org/10.1016/0025-3227(90)90114-Y

Gačić M., Mancero Mosquera I., Kovačević V., et al. 2004. Temporal variations of water flow between the Venetian lagoon and the open sea. J. Mar. Syst. 51: 33-47. https://doi.org/10.1016/j.jmarsys.2004.05.025

Grifoll M., Del Campo A., Espino M., et al. 2011. Water renewal and risk assessment of water pollution in semi-enclosed domains: Application to Bilbao Harbour (Bay of Biscay). J. Mar. Syst. 109-110: S241-S251. https://doi.org/10.1016/j.jmarsys.2011.07.010

Grifoll M., Jordà G., Sotillo M.G., et al. 2012. Water circulation forecasting in Spanish harbours. Sci. Mar. 76: 45-61. https://doi.org/10.3989/scimar.03606.18B

Grifoll M., Navarro J., Pallarès E., et al. 2016. Ocean-atmosphere-wave characterisation of a wind jet (Ebro shelf, NW Mediterranean Sea). Nonlin. Processes Geophys. 23: 143-158. https://doi.org/10.5194/npg-23-143-2016

Hagy J.D., Sanford L.P., Boynton W.R. 2000. Estimation of net physical transport and hydraulic residence times for a coastal plain estuary using box models. Estuaries 23: 328-340. https://doi.org/10.2307/1353325

Hansen D.V., Rattray M. 1965. Gravitational circulation in straits and estuaries. J. Mar. Res. 22: 104-122.

Huang N.E., Shen Z., Long S.R., et al. 1998. The empirical mode decomposition and the Hilbert spectrum for nonlinear and non-stationary time series analysis. Proc. R. Soc. A Math. Phys. Eng. Sci. 454: 903-995. https://doi.org/10.1098/rspa.1998.0193

Janzen C., Wong K. 1998. On the low-frequency transport processes in shallow coastal lagoon. Estuaries 21: 754-766. https://doi.org/10.2307/1353279

Large W.G., Pond S. 1981. Open-ocean momentum flux measurements in moderate to strong winds. J. Phys. Oceanogr. 11: 324-336. https://doi.org/10.1175/1520-0485(1981)011<0324:OOMFMI>2.0.CO;2

Llebot C. 2010. Interactions between physical forcing, water circulation and phytoplankton dynamics in a microtidal estuary. PhD thesis, Univ. Las Palmas de Gran Canaria, Islas Canarias, Spain.

Llebot C., Solé J., Delgado M., et al. 2011. Hydrographical forcing and phytoplankton variability in two semi-enclosed estuarine bays. J. Mar. Syst. 86: 69-86. https://doi.org/10.1016/j.jmarsys.2011.01.004

Llebot C., Rueda F.J., Solé J., et al. 2013. Hydrodynamic states in a wind-driven microtidal estuary (Alfacs Bay). J. Sea Res. 85: 263-276 https://doi.org/10.1016/j.seares.2013.05.010

Malačič V., Petelin B. 2009. Climatic circulation in the Gulf of Trieste (northern Adriatic). J. Geophys. Res. Oceans 114. https://doi.org/10.1029/2008JC004904

Martín Vide J. 2005. Los mapas del tiempo, Vol.1 de Colección Geoambiente XXI. Davinci Continental, Ed. Davinci, Mataró, Barcelona, 219 pp.

Monismith S. 1986. An experimental study of the upwelling response of stratified reservoirs to surface shear stress. J. Fluid. Mech. 171: 407-439. https://doi.org/10.1017/S0022112086001507

Murphy P.L., Valle-Levinson A. 2008. Tidal and residual circulation in the St. Andrew Bay system, Florida. Cont. Shelf Res. 28: 2678-2688. https://doi.org/10.1016/j.csr.2008.09.003

Narváez D.A., Valle-Levinson A. 2008. Transverse structure of wind-driven flow at the entrance to an estuary: Nansemond River. J. Geophys. Res. Oceans 113: 1-9. https://doi.org/10.1029/2008JC004770

Noble M.A., Schroeder W.W., Wiseman W.J., et al. 1996. Subtidal circulation patterns in a shallow, highly stratified estuary Mobile Bay, Alabama. J. Geophys. Res. 101: 25689-25703. https://doi.org/10.1029/96JC02506

Pritchard D.W. 1952: Salinity distribution and circulation in the Chesapeake Bay estuarine system. J. Mar. Res. 11: 106-123.

Pritchard D.W, Kent R.E. 1956. A Method of Determining Mean Longitudinal Velocities in a Coastal Plain Estuary. J. Mar. Res. 15: 81-91.

Salas-Monreal D., Valle-Levinson A. 2008. Sea-Level Slopes and Volume Fluxes Produced by Atmospheric Forcing in Estuaries: Chesapeake Bay Case Study. J. Coast. Res. 2: 208-217. https://doi.org/10.2112/06-0632.1

Schaeffer A., Garreau P., Molcard A., et al. 2011. Influence of high-resolution wind forcing on hydrodynamic modeling of the Gulf of Lions. Ocean Dyn. 61: 1823-1844. https://doi.org/10.1007/s10236-011-0442-3

Shchepetkin A., McWilliams J., 2005. The regional oceanic modeling system(ROMS): a split-explicit, free-surface, topography-following-coordinate oceanic model. Ocean. Model. 9: 347-404. https://doi.org/10.1016/j.ocemod.2004.08.002

Solé J., Turiel A., Estrada M., et al. 2009. Climatic forcing on hydrography of a Mediterranean bay (Alfacs Bay). Cont. Shelf Res. 29: 1786-1800. https://doi.org/10.1016/j.csr.2009.04.012

Uncles R.J., Stephens J.A., Harris C. 2014. Estuarine, Coastal and Shelf Science. Estuar. Coast. Mar. Sci. 150: 242-251. https://doi.org/10.1016/j.ecss.2014.04.019

Valle-Levinson A., Blanco L. 2004. Observations of wind influence on exchange flows in a strait of the Chilean Inland Sea. J. Mar. Res. 62: 721-741. https://doi.org/10.1357/0022240042387565

Valle-Levinson A., Delgado J.A., Atkinson L.P. 2001. Reversing Water Exchange Patterns at the Entrance to a Semiarid Coastal Lagoon. Estuar. Coast. Shelf Sci. 53: 825-838. https://doi.org/10.1006/ecss.2000.0813

Valle-Levinson A., Mariño-Tapia I., Enriquez C., et al. 2011. Tidal variability of salinity and velocity fields related to intense point-source submarine groundwater discharges into the coastal ocean. Limnol. Oceanogr. 56: 1213-1224. https://doi.org/10.4319/lo.2011.56.4.1213

Van Maren D., Hoekstra P. 2004. Seasonal variation of hydrodynamics and sediment dynamics in a shallow subtropical estuary: the Ba Lat River, Vietnam. Estuar. Coast. Shelf Sci. 60: 529-540. https://doi.org/10.1016/j.ecss.2004.02.011

Wong K.-C., Valle-Levinson A. 2002. On the relative importance of the remote and local wind effects on the subtidal exchange at the entrance to the Chesapeake Bay. J. Mar. Res. 60: 477-498. https://doi.org/10.1357/002224002762231188